

Line edge roughness metrology using atomic force microscopes

Ndubuisi G Orji¹, Theodore V Vorburger¹, Joseph Fu¹,
Ronald G Dixson¹, Cattien V Nguyen² and Jayaraman Raja³

¹ National Institute of Standards and Technology, Gaithersburg, MD 20899-8212, USA

² ELORET Corp./NASA Ames Research Center, Moffett Field, CA 94033, USA

³ University of North Carolina at Charlotte, Charlotte, NC 28223, USA

Abstract

Line edge roughness (LER) measurements using two types of atomic force microscopes and three types of tips are compared. Measurements were made on specially prepared samples with inscribed edge roughness of different amplitudes and wavelengths. The spatial wavelengths and amplitudes each instrument was able to measure are compared. Techniques on checking the noise level of LER measuring instruments are highlighted.

Keywords: atomic force microscope, line edge roughness, carbon nanotube

Introduction

Over the years, the size of components that make up microelectronics integrated circuits (IC) has steadily decreased. A key measure of the size of features used to fabricate IC components is the width of patterned lines. The relative uncertainty associated with determining the width of these lines has increased, as the width itself decreases. A major source of this uncertainty is the deviation of the line edge from a straight line, otherwise known as line edge roughness (LER). LER has been linked to current leakage [1] and voltage fluctuations [2, 3] in devices, and is becoming an important contributor to the lithography error budget. The tools currently used to measure LER have limitations and may not be able to meet the LER measurement needs of the semiconductor industry. This is because semiconductor lines are complex three-dimensional structures with vertical surfaces and the available instruments are not optimized for such measurement. The definition of LER used in this paper refers strictly to the edge of a line feature as illustrated in figure 1. The International Technology Roadmap for Semiconductors (ITRS) [4] specifies a requirement of 3 nm for LER for the year 2004 and smaller values for subsequent years. These specifications are close to the spatial resolution of most instruments used to characterize LER, so the noise level of the instruments could be a factor. Hence, there is a need for robust LER metrology techniques. An earlier metrology study of instruments for measuring LER was conducted by

Nelson *et al* [5], where they concentrated mainly on differences between atomic force microscopes (AFMs) and scanning electron microscopes (SEMs). Other groups focused on understanding the origins of LER in resist material and the influence of processing conditions (Hinsberg *et al* [6], Somervell *et al* [7] and Patsis *et al* [8], for example).

The AFM, with spatial resolution approaching the atomic scale for measurements of smooth surfaces [9], is the only instrument with the capability of achieving the LER requirements specified in the ITRS. However, the slow speed of the AFM relative to the SEM mitigates this advantage. Furthermore, there are several types of AFMs and AFM tips and it is not clear if they measure edge roughness in the same way. We studied the use of the AFM for LER measurements, with emphasis on differences obtained when using various types of AFMs. We used two types of AFMs and three types of tips to evaluate a set of prototype LER samples. The samples were designed to have square-wave structures with different amplitudes and spatial wavelengths. This deterministic design allows one to determine the sizes of features each instrument configuration can characterize. The study emphasizes the measurement procedures needed to obtain LER metrology information with the different types of AFM configurations used. The study also highlights the differences in results obtained both by the instruments and by the tips used, and the type of evaluation needed to assess the noise level of probe instruments for LER measurements. For an overview of AFM-based LER measurements, see Orji *et al* [10].

Preprint

see {NG Orji, RG Dixson 2005 *Meas. Sci. Technol.* 16 2147} for final version

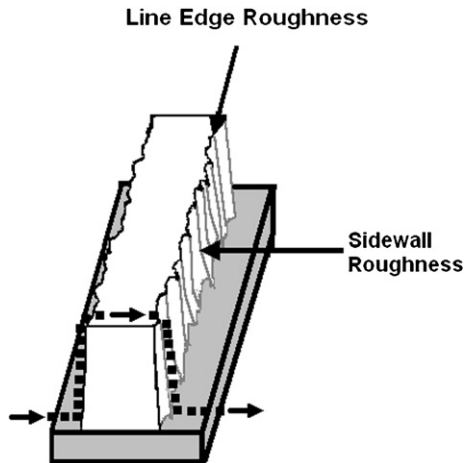


Figure 1. Schematic diagram of a patterned line feature. LER refers only to the roughness at the edge of the line feature. The arrow indicates the scan direction.

Tools

Two types of AFMs were used in this study, a conventional AFM and a critical-dimension (CD) AFM. The conventional AFM [11] images surfaces in a top-down fashion and height data are obtained at fixed x and y locations. This is the most widely used type of AFM. The tapping-mode[®] implementation of the conventional AFM was used in this experiment⁴. The CD-AFM is a specialized instrument that can measure vertical surfaces in addition to horizontal surfaces [12]. The instrument operates in two modes: in top-down mode and in CD mode. When operating in the CD mode, the instrument can directly access and measure the sidewall of patterned line features. For this experiment, although the information extracted and evaluated is the LER as illustrated in figure 1, rather than the sidewall data. During contact with the sidewall, x data are acquired at different z locations. The calibrations of both instruments were verified using well-characterized samples. The dashed lines in figure 1 show the profiling direction for both instruments.

The three types of tips used were a conventional (CONV) AFM tip, a carbon nanotube (CNT) fitted tip and a CD-AFM tip (also known as a boot-shaped or flared tip). The conventional tip and the nanotube-fitted tip were used with the conventional AFM, while the boot-shaped tip was used with the CD-AFM. The carbon nanotube was attached to the cantilever by creating a dc current between the tip and a cartridge containing scores of nanotubes deposited by chemical vapour deposition as described by Stevens *et al* [13]. An SEM image of the CNT tip used is shown in figure 2. Boot-shaped tips are specially designed to access feature sidewalls. A schematic diagram of a boot-shaped tip is shown in figure 3.

The samples used in this study were designed and fabricated by SEMATECH to have square-wave features in a variety of sizes [14]. There were two types of samples,

⁴ Certain commercial equipment is identified in this paper to adequately describe the experimental procedure. Such identification does not imply recommendation or endorsement by the National Institute of Standards and Technology, nor does it imply that the equipment identified is necessarily the best available for the purpose.

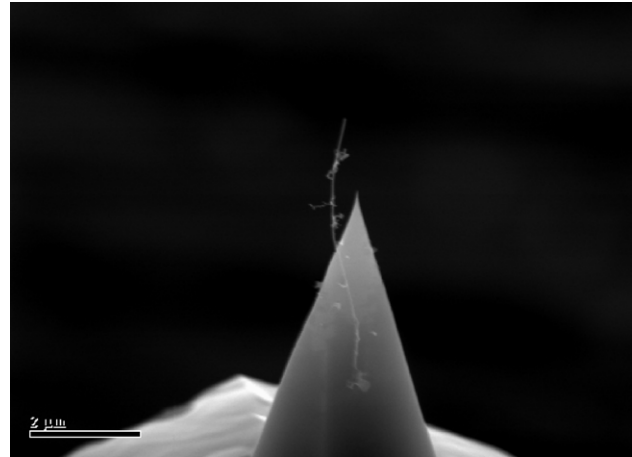


Figure 2. SEM image of the carbon nanotube tip used.

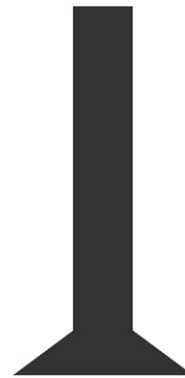


Figure 3. Schematic diagram of a boot-shaped tip.

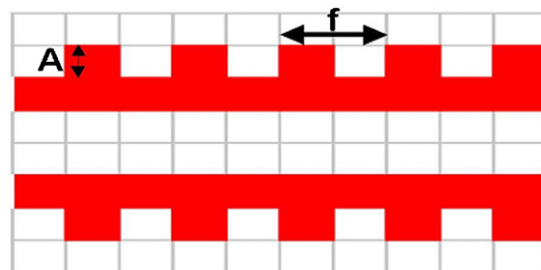


Figure 4. Schematic diagram of the sample design. A indicates the amplitude, while f indicates the spatial wavelength.

one having features etched in photoresist material and another etched in polycrystalline silicon. A schematic diagram of the sample design is shown in figure 4, where A represents the amplitude and f represents the spatial wavelength. The design includes two nominal amplitudes, 50 nm and 100 nm, and nine spatial wavelengths ranging from 50 nm to 800 nm.

Measurements

Three spatial wavelengths were selected for measurement for both the resist and polysilicon samples. Figure 5 shows an overview of the measurements, which included three instruments, two types of samples, two feature amplitudes and

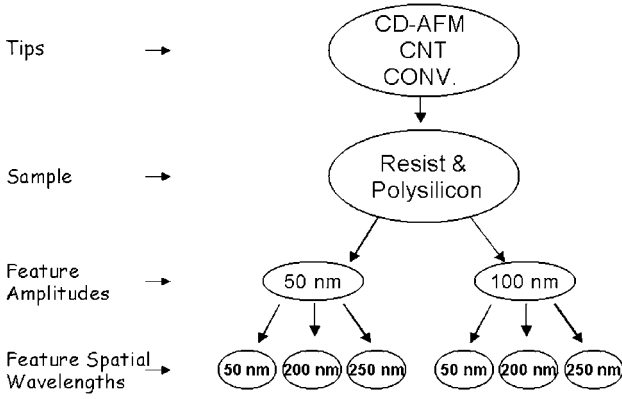


Figure 5. An overview of the tools, sample and feature sizes evaluated.

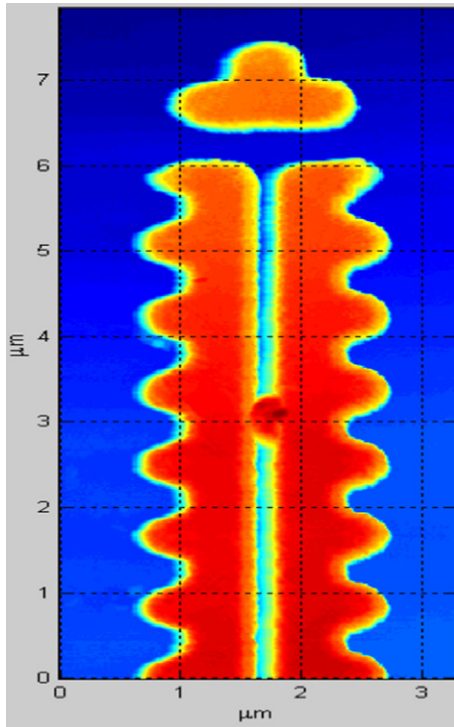


Figure 6. Top-down image of one of the line features. The spatial wavelength for the inscribed edge features is 800 nm. This particular feature has a larger amplitude than those used in the analysis, however, it clearly shows the periodic nature of the features.

for each amplitude, three spatial wavelengths for a total of six sites per sample. To help neutralize systematic effects if any, the conventional AFM measurements were randomized with respect to tip and sample type. The CD-AFM measurements were randomized with respect to sample type because the CD-AFM accepts one type of tip. The conventional AFM acquired data in a raster scan while the CD-AFM acquired data in a boustrophedon manner. Figure 6 shows a top-down image of a resist sample acquired using a conventional AFM. This particular feature, which includes compound square-wave structures, has a larger amplitude than the features used in the analyses; however, it clearly shows the periodic nature of the design.

Table 1. Measurement spatial frequency range.

Feature spatial wavelength (nm)	Feature spatial frequency (μm^{-1})	CD-AFM (μm^{-1})	CONV (μm^{-1})	CNT (μm^{-1})
50	20	1–50	1–256	1–256
200	5	0.5–50	0.5–128	0.5–128
250	4	0.5–62	0.5–128	0.5–128

Analysis and results

Edge profiles were extracted from the images for analysis using a fitting-based approach. For the CD-AFM data, a second-order polynomial least-squares fit that models the undercut profiles and used both the z -axis data and the x -axis data from the CD-AFM was used. The detailed algorithm is described elsewhere [15]. The edges in the conventional AFM data were extracted by fitting a second-order polynomial least-squares curve to the edge and selecting locations that matched the maximum difference (left edge) and minimum difference (right edge) of the data. Fitting-based edge detection methods have been shown to be less susceptible to noise [14]. After extracting the edge profile, a least-squares line was removed from the data. This is the only pre-processing of the data before analysis. Figure 7(a) shows an image of a 250 nm spatial wavelength polysilicon image, while figure 7(b) shows the corresponding edge profiles. The Rq values of each of the profiles were calculated using the formula in equation (1), where z_i represents discrete data points and N is the number of data points.

$$\text{Rq} = \left(\frac{1}{N} \sum_i^N (z_i)^2 \right)^{1/2}. \quad (1)$$

The spatial frequency ranges over which the Rq values were calculated are shown in table 1. Figure 8(a) shows the Rq results for both the nominal 50 nm and 100 nm amplitude resist features, while figure 8(b) shows results for the same parameters for the polysilicon sample. At the nominal 50 nm amplitude, no single instrument could be said to have values that are clearly larger or smaller than the others in all the feature spatial wavelengths measured. An interesting observation is the range of values measured by each of the instruments across the three sample sizes. The ranges of peak-to-valley (Rt)(figures 9(a) and (b)) results were highest for the CNT tip for both the resist (18.81 nm) and polysilicon (15.31 nm) 250 nm spatial wavelength samples. The 250 nm spatial wavelength samples generally had the highest peak-to-valley values. This is attributed to the ability of the tip to access the valleys of the sinusoidal structures with larger spacing. Only the CD-AFM results for resist and polysilicon nominal 50 nm amplitude conflict with this observation; re-measurement of these resist features with the CD-AFM confirmed this observation. It must be pointed out that the intended square-wave design of the samples did not resolve, as shown by figure 6, the features are closer to sine waves than square waves. The amplitudes reported here are also smaller, this is probably due to the fabrication process because the results are in qualitative agreement with SEM image results.

For the nominal 100 nm amplitude features, with the exception of a few places, the Rq and Rt values increased

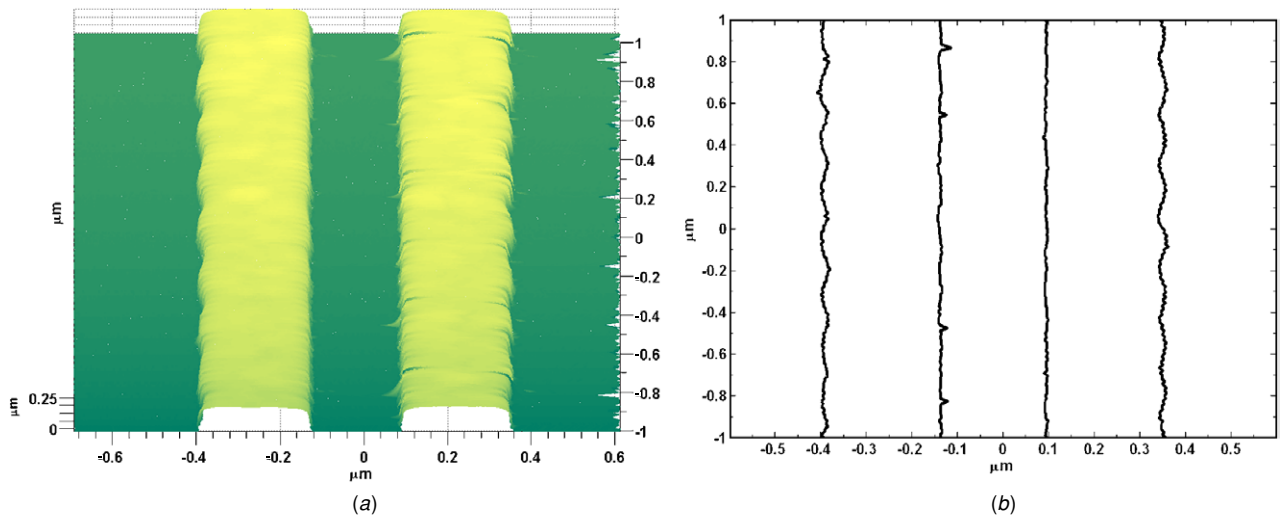


Figure 7. Examples of edge profiles extracted from the images. (a) CD-AFM image of polysilicon line features. (b) Edge profiles extracted from the image in (a).

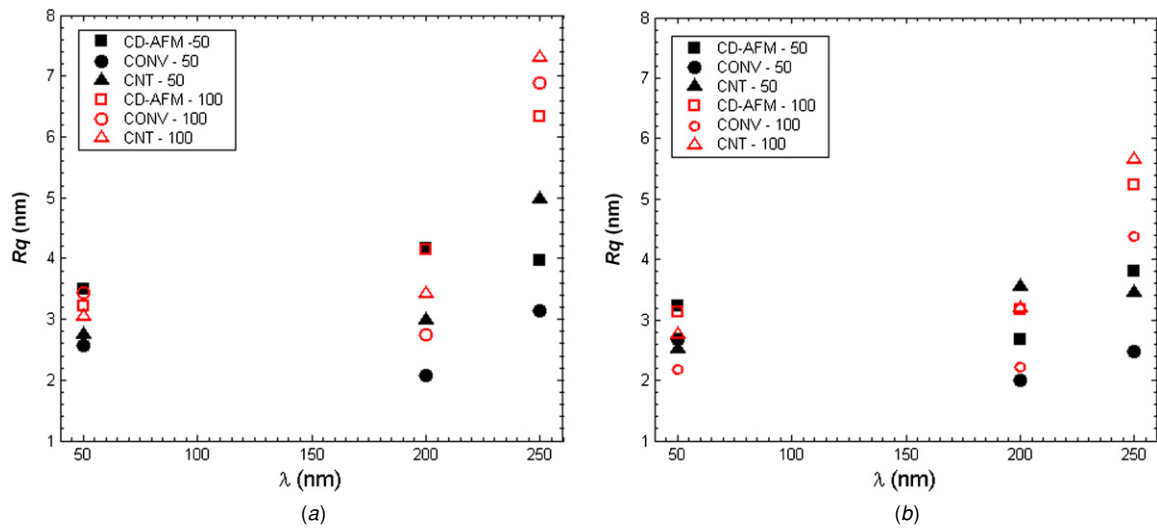


Figure 8. R_q results for 50 nm, 200 nm and 250 nm spatial wavelength features etched in (a) photoresist material and (b) polysilicon material.

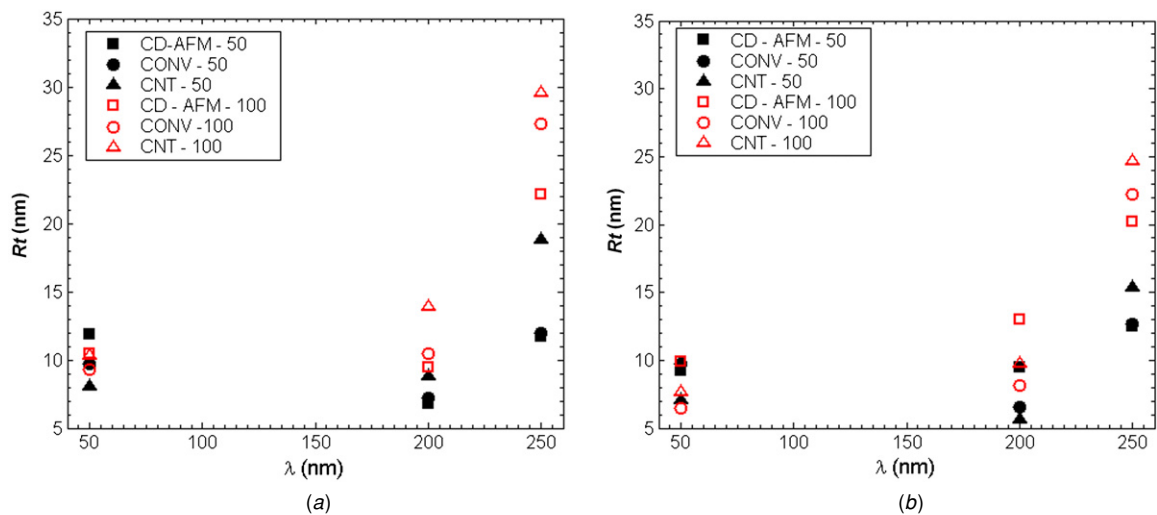


Figure 9. Peak-to-valley results for 50 nm, 200 nm and 250 nm spatial wavelength features etched in (a) photoresist material and (b) polysilicon material.

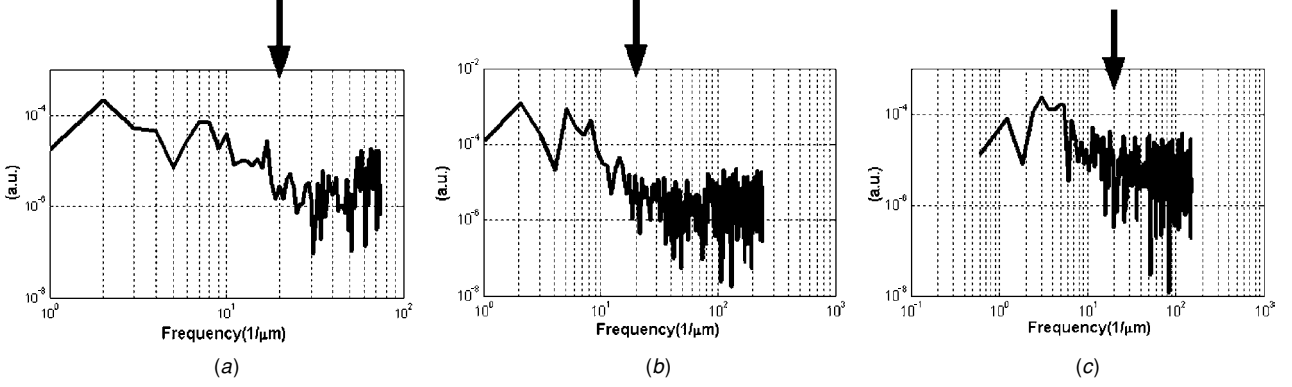


Figure 10. Representative PSD plots from images obtained with (a) the CD-AFM tip, (b) the CONV tip and (c) the CNT tip. The features are nominal 50 nm amplitude and 50 nm spatial wavelength polysilicon sample. The arrows represent the intended design locations of the main peak.

with spatial wavelength for each method for both resist and polysilicon. For the resist, the CNT tip gave the highest Rt values for the 200 nm and 250 nm spatial wavelength resist samples followed by the CONV tip. At 100 nm amplitude, all the values increased between a spatial wavelength of 200 nm and a spatial wavelength of 250 nm. Also, for the 250 nm spatial wavelength, the Rt and Rq change systematically with imaging method. The CD-AFM tip had the lowest, while the CNT tip had the largest values. We attribute this to the increased resolution of the CNT tip and the possibility that the lithography resolved better with increased feature spacing. The Rq and Rt results for the 50 nm amplitude samples did not clearly show higher or lower values for any of the methods. The CD-AFM with its large radius tip was not able to adequately characterize the low spatial wavelength features. Smaller tip sizes will be required if one intends to use the CD-AFM to characterize LER with spatial wavelength of 200 nm and below.

We also calculated the power spectral densities (PSD) of the profiles. The PSD decomposes the surface profile into its various Fourier components and may be defined by equation (2) in analytical form and equation (3) in discrete form.

$$\text{PSD}(F) = \lim_{L \rightarrow \infty} \left(\frac{1}{L} \right) \left| \int_{-L/2}^{L/2} z(x) e^{-2i\pi Fx} dx \right|^2, \quad (2)$$

$$\text{PSD}(F) = \frac{\Delta}{N} \left| \sum_{j=1}^N z(j) e^{-2i\pi F(j-1)\Delta} \right|^2, \quad (3)$$

where F represents the spatial frequency, Δ is the sampling interval, j is an index and $i = \sqrt{-1}$. Figure 10 shows representative PSD plots for the 50 nm spatial wavelength. The arrows on all of the PSD plots indicate the locations of the designed feature spatial wavelength. None of the techniques were able to resolve the 50 nm spatial wavelength features. Some of the dominant spatial frequencies present in the PSD plots could be due to instrument noise rather than the feature spatial frequency of interest. For example, figure 10(a)(CD-AFM PSD plots) shows a peak around 100 nm spatial wavelength. However, the tip used is approximately 117 nm across and may have averaged edge deviations less than the size

of the tip. As Nelson *et al* [5] pointed out, the Rq roughness values obtained using boot-shaped tips that are much larger than the spatial wavelength likely do not represent the actual edge roughness of the sample. Boot-shaped tips as small 70 nm are commercially available [16], but are not compatible with the specific instrument used.

Figure 11 shows representative PSD plots for the 200 nm spatial wavelength features. The CNT tip was the only technique able to resolve the 200 nm spatial wavelength features as shown by the location of the peaks in figure 11(c); the PSD plots for the CD-AFM and CONV tips show no such peaks. All the methods were able to image the 250 nm spatial wavelength features as shown by the PSD plots in figure 12. This is true for both the nominal 50 nm and 100 nm amplitude features, and also for both resist and polysilicon etched samples.

Noise resolution

The metrology requirements specified for LER in the ITRS are close to the noise resolution of the AFM instruments used here to measure LER. For such measurements to be meaningful, it is important to ascertain the noise floor of the instruments. We evaluated the noise levels of the instruments by measuring the non-inscribed side of the 50 nm spatial wavelength and 50 nm nominal amplitude resist feature. The Rq values are 1.61 nm for the CD-AFM, 1.81 nm for the CONV tip and 2.05 nm for the CNT tip, obtained over the spatial frequency ranges listed in table 1. The above values indicate that all our LER results are above the noise levels of the specific instruments we used. It is important to note that the different instruments are not being compared here, rather the objective is to see if each instrument obtains a lower Rq when measuring a smoother edge. Also, these values may not represent the ultimate lateral noise level of the instrument. The Rq values are comprised of contributions from the feature edge, the instrument noise and the environment. These are not easily separable, but the smoother the sample, the better indication one will have of the instrument noise. For these types of measurements where the expected values are close to the instrument noise, this is a valuable test to perform if one has access to suitable samples. The values

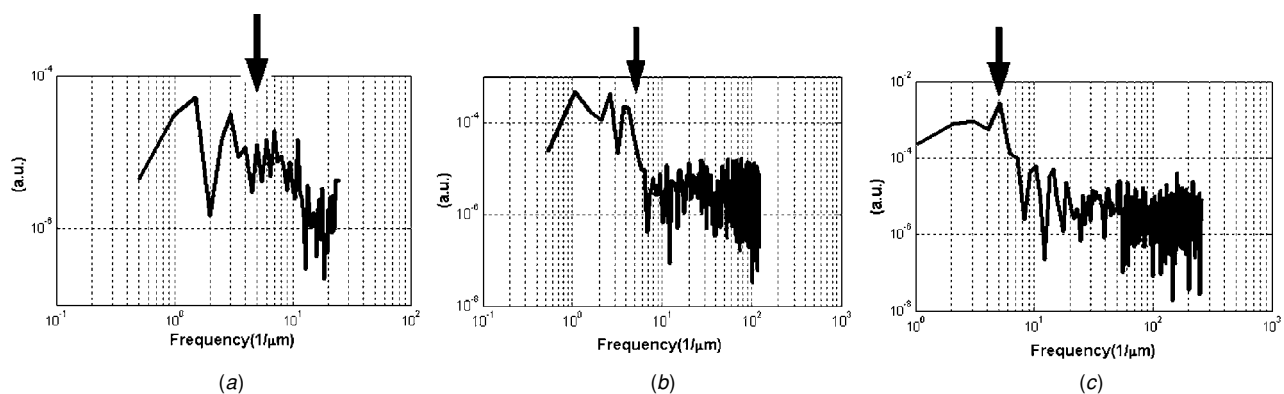


Figure 11. Representative PSD plots from images obtained with (a) the CD-AFM tip, (b) the CONV tip and (c) the CNT tip. The features are nominal 100 nm amplitude and 200 nm spatial wavelength resist sample.

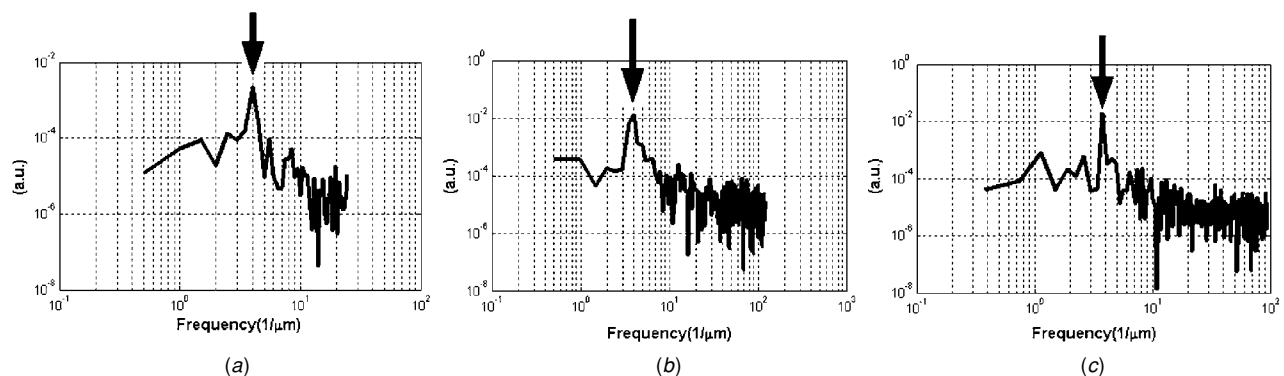


Figure 12. Representative PSD plots from images obtained with (a) the CD-AFM tip, (b) the CONV tip and (c) the CNT tip. The features are nominal 100 nm amplitude and 250 nm spatial wavelength resist sample.

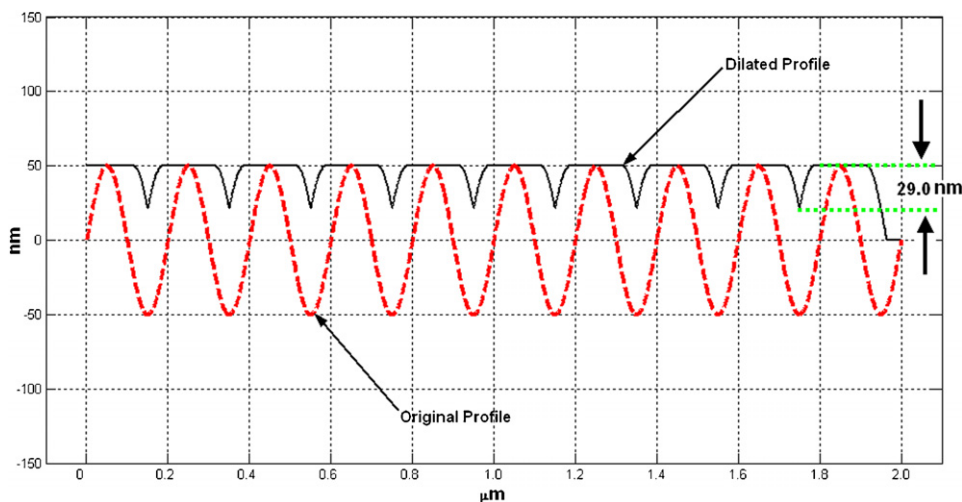


Figure 13. A simulated 200 nm spatial wavelength sine profile, and the dilated profile produced when measured by a 117 nm boot-shaped tip.

will indicate the noise level one would expect to get when measuring the types of samples used for the test. One can also acquire images with a zero scan size, here the noise could be from the instrument and/or the environment. Power spectral density analysis of the data will reveal the frequency of the signals, which could then be matched to a noise source and addressed.

Discussion

Based on the location of the peaks in the PSD plots in figures 10–12, all the techniques were able to characterize the largest feature spatial wavelength measured (250 nm). The data and analyses clearly show that the conventional AFM fitted with carbon nanotube tips has better resolution than the

CD-AFM and the conventional AFM with conventional tips. The CD-AFM tip and the conventional tip were not able to resolve features with 200 nm in spatial wavelength. The CD-AFM tip was ≈ 117 nm across and most likely dilated the output data [17–19]. Figure 13 shows a simple morphological model of a sinusoidal profile of 200 nm spatial wavelength and 100 nm peak-to-valley, dilated by a flat tip of 117 nm across; the final profile shows a decrease in the peak-to-valley by over 70%. Tip influence such as this probably accounts for some of the attenuation of the peak-to-valley. As mentioned earlier, for newer generation CD-AFMs, boot-shaped tips as small as 70 nm across are commercially available [16], and the use of tips as small as 32 nm has been reported [20]. The unavailability of even smaller CD-AFM tips makes it a poor choice for high-frequency LER measurements because of the very stringent requirements specified in the ITRS. However, it was able to resolve the 250 nm spatial wavelength, so it could be used in measurements where low-frequency roughness is of interest. The CD-AFM is a useful instrument if direct sidewall profiling is needed, but it will reach its full potential with improvements in tip size and characterization. Research in the use of carbon nanotubes on boot-shaped tips is ongoing and, if successful, will dramatically increase the resolution of the instrument.

The CNT tip was able to resolve the 200 nm spatial wavelength features. This is interesting because it was used in the same instrument as the conventional tip, which indicates that the differences in the results are entirely due to the tip. Special attention should be paid to the instrument scan rate when using the CNT tip because it could flex during measurement. The flex motion of CNT tip may be minimized by using shorter length CNT. The slightly higher values obtained with the CNT tip during the noise resolution test could be an indication of noise. Another area that could improve LER measurements is the use of standard samples. The results in figure 9 show that the lithography attenuated the nominal amplitude values. Using standard samples will enable instrument makers and users to quickly determine what features their instruments can measure and also as check standards for process control. The samples used in this study are a good start and their design could form the basis of such a standard. This will include not just physical standards, but also standardization of measurement procedures and analysis techniques. The procedure specified by the ITRS on how to assess LER is another good start and one that should be built on.

Conclusion

The control, specification and measurement of LER is a new field with many research issues in play with large technological and economic implications. The AFM because of its resolution has the ability to characterize LER down to the levels specified in the ITRS. Concerns such as throughput (which was not addressed here) may limit situations where it could be used. However, using the AFM to study LER could lead to insights on how to control LER. The above study shows that there are differences on how the various AFMs measure LER, and outlines certain considerations that users should bear in mind when using each technique.

Acknowledgments

This work was partially funded by the Office of Microelectronics Programs (OMP) at NIST. Benjamin Bunday of SEMATECH supplied the samples. CVN is supported through a subcontract from University Affiliated Research Center at NASA Ames operated by University of California, Santa Cruz. The authors are grateful to Andras Vladar and Jack Martinez of NIST for useful comments and discussions.

References

- [1] Diaz C H, Tao H J, Ku Y C, Yen A and Young K 2001 An experimentally validated analytical model for gate line-edge roughness (LER) effects on technology scaling *IEEE Electron Device Lett.* **22** 287–9
- [2] Asenov A, Kaya S and Brown A R 2003 Intrinsic parameter fluctuations in decanometer MOSFETs introduced by gate line edge roughness *IEEE Trans. Electron Devices* **50** 1254–60
- [3] Patterson K, Sturtevant J L, Alvis J, Benavides N, Bonser D, Cave N, Nelson-Thomas C, Taylor B and Turnquest K 2001 Experimental determination of the impact of polysilicon LER on sub-100-nm transistor performance *Proc. SPIE* **4344** 809–14
- [4] *International Technology Roadmap for Semiconductors (ITRS) 2003* Semiconductor Industry Association, San Jose, CA
- [5] Nelson C, Palmateer S C, Forte A R and Lyszczarz T M 1999 Comparison of metrology methods for quantifying the line edge roughness of patterned features *J. Vac. Sci. Technol. B* **17** 2488–98
- [6] Hinsberg W, Houle F A, Hoffnagle J, Sanchez M, Wallraff G, Morrison M and Frank S 1998 Deep-ultraviolet interferometric lithography as a tool for assessment of chemically amplified photoresist performance *J. Vac. Sci. Technol. B* **16** 3689–94
- [7] Somervell M H, Fryer D S, Osborn B, Patterson K, Byers J and Willson C G 2000 Study of the fundamental contributions to line edge roughness in a 193 nm, top surface imaging system *J. Vac. Sci. Technol. B* **18** 2551–9
- [8] Patsis G P, Tserepi A, Raptis I, Glezos N, Gogolides E and Valamontes E S 2000 Surface and line-edge roughness in solution and plasma developed negative tone resists: experiment and simulation *J. Vac. Sci. Technol. B* **18** 3292–6
- [9] Rugar D and Hansma P 1990 Atomic force microscopy *Phys. Today* **43** 23–30
- [10] Orji N G, Sanchez M I, Raja J and Vorbuerger T V 2004 AFM characterization of semiconductor line edge roughness, In *Applied Scanning Probe Methods* ed B Bhushan, H Fuchs and S Hosaka (Berlin: Springer) pp 277–301 DOI: 10.1007/978-3-642-35792-3_9
- [11] Binnig G, Quate C F and Gerber C 1986 Atomic force microscope *Phys. Rev. Lett.* **56** 930–3
- [12] Martin Y and Wickramasinghe H K 1994 Method for imaging sidewalls by atomic force microscopy *Appl. Phys. Lett.* **64** 2498–500
- [13] Stevens R, Nguyen C, Cassell A, Delzeit L, Meyyappan M and Han J 2000 Improved fabrication approach for carbon nanotube probe devices *Appl. Phys. Lett.* **77** 3453–5
- [14] Bunday B, Bishop M, Villarrubia J S and Vladar A 2003 CD-SEM measurement of line edge roughness test patterns for 193 nm lithography *Proc. SPIE* **5038** 674–88
- [15] Orji N G 2004 *PhD Thesis* University of North Carolina at Charlotte, Charlotte, NC
- [16] *Veeco Probes Catalog* 2004 Veeco Instruments LLC, Santa Barbara, CA
- [17] Villarrubia J S 1997 Algorithms for scanned probe microscope image simulation, surface reconstruction, and tip estimation *J. Res. Natl Inst. Stand. Technol.* **102** 425–54

- [18] Chen Y and Huang W 2004 Numerical simulation of the geometrical factors affecting surface roughness measurements by AFM *Meas. Sci. Technol.* **15** 2005–10
- [19] Dai G, Jung L, Pohlenz F, Danzebrink H, Kruger-Sehm R, Hasche K and Wilkening G 2004 Measurement of micro-roughness using a metrological large range scanning force microscope *Meas. Sci. Technol.* **15** 2039–46
- [20] Foucher J 2005 From CD to 3D sidewall roughness analysis with 3D CD-AFM *Proc. SPIE* **5752** 966–76